PHYSICAL REVIEW B **98**, 060401(R) (2018)

Rapid Communications

Fluctuation-induced Néel and Bloch skyrmions at topological insulator surfaces

Flavio S. Nogueira,[1,2] Ilya Eremin,[2,3] Ferhat Katmis,[4,5] Jagadeesh S. Moodera,[4,6] Jeroen van den Brink,[1,7] and Volodymyr P. Kravchuk[1,8]

[1]*Institute for Theoretical Solid State Physics, IFW Dresden, Helmholtzstraße 20, DE-01069 Dresden, Germany*
[2]*Institut für Theoretische Physik III, Ruhr-Universität Bochum, Universitätsstraße 150, DE-44801 Bochum, Germany*
[3]*National University of Science and Technology MISiS, 119049 Moscow, Russia*
[4]*Francis Bitter Magnet Laboratory and Plasma Science and Fusion Center, Massachusetts Institute of Technology, Cambridge, Massachusetts 02139, USA*
[5]*Department of Physics, Middle East Technical University, TR-06800 Ankara, Turkey*
[6]*Department of Physics, Massachusetts Institute of Technology, Cambridge, Massachusetts 02139, USA*
[7]*Institute for Theoretical Physics, TU Dresden, DE-01069 Dresden, Germany*
[8]*Bogolyubov Institute for Theoretical Physics of National Academy of Sciences of Ukraine, 03680 Kyiv, Ukraine*

(Received 20 April 2018; published 3 August 2018)

Ferromagnets in contact with a topological insulator have become appealing candidates for spintronics due to the presence of Dirac surface states with spin-momentum locking. Because of this, bilayer Bi_2Se_3-EuS structures, for instance, show a finite magnetization at the interface at temperatures well exceeding the Curie temperature of bulk EuS. Here, we determine theoretically the effective magnetic interactions at a topological insulator-ferromagnet interface *above* the magnetic ordering temperature. We show that by integrating out the Dirac fermion fluctuations an effective Dzyaloshinskii-Moriya interaction and magnetic charging interaction emerge. As a result, individual magnetic skyrmions and extended skyrmion lattices can form at the interfaces of ferromagnets and topological insulators, the first indications of which have been very recently observed experimentally.

DOI: 10.1103/PhysRevB.98.060401

Introduction. The spin-momentum locking property of three-dimensional topological insulators (TIs) [1,2] makes them promising candidate materials for future spin-based electronic devices. One important consequence of spin-momentum locking in TIs is the topological electromagnetic response, which arises from induced Chern-Simons (CS) terms [3] on each surface [4]. This happens, for instance, when time-reversal (TR) symmetry is broken, which renders the surface Dirac fermions gapped. This can be achieved, for example, by a proximity effect with a ferromagnetic insulator (FMI) [5–15]. In this case, a CS term is generated if there are an odd number of *gapped* Dirac fermions, which is achieved only in the presence of out-of-plane exchange fields [11]. The realization of several physical effects related to the CS term that have been predicted in the literature critically depends on growing technologies required for the fabrication of heterostructures involving both strong TIs and FMIs. Recently, high-quality Bi_2Se_3-EuS bilayer structures have been shown to exhibit proximity-induced ferromagnetism on the surface of Bi_2Se_3 [6,16,17]. Other successful realizations of stable ferromagnetic TI interfaces were demonstrated recently [18,19]. In addition, it was shown that the interface of FMI and TI can have a magnetic ordering temperature much higher than the bulk ordering temperature [5], indicating that topological surface states can strongly affect the magnetic properties of a proximity-coupled FMI.

These experimental advances motivate us to investigate the effective magnetic interactions that result from the fluctuating momentum-locked Dirac fermion surface states of a TI in contact with an FMI.

We show that even in the absence of any spontaneous magnetization, at temperatures above the Curie temperature of the FMI, intriguing topologically stable magnetic textures, i.e., skyrmions, are induced as a result of quantum fluctuations of the Dirac fermions at the interface. In fact, we demonstrate that integrating out Dirac fermions coupled to a FMI thin film generates a Dzyaloshinskii-Moriya interaction (DMI), that, depending on the form of the Dirac Hamiltonian, favors either Néel- or Bloch-type skyrmions [20–23]. However, skyrmions induced in TI-FMI structures feature in addition a "charging energy," due to the generation of a term proportional to the square of the so-called magnetic charge $\nabla \cdot \mathbf{n}$, where $\mathbf{n}$ denotes the direction of the magnetization [24]. An important feature of our finding is that the Dirac fermions that are integrated out *are not gapped*, since there is no spontaneous magnetization above T_c that would lead to a gap in the Dirac spectrum. Furthermore, the generated DMI is only nonzero if the chemical potential does not vanish. We obtain the phase diagram for the skyrmion solutions and identify the region of stability for skyrmion lattices in the presence of the magnetic charging energy. We determine this region numerically by analyzing the excitation spectrum of the skyrmion solution. An important discovery is that the magnetic charging energy modifies the phase diagram significantly in the case of DMIs favoring Néel skyrmions, a situation relevant for Bi_2Se_3-EuS interfaces. Our theoretical findings support conceptually the recent experimental observation of a skyrmion texture at a ferromagnetic heterostructure of Cr-doped Sb_2Te_3 [19]. Having a skyrmion profile on a TI surface will cause significant changes in the conductance that may be observed in transport measurements [25].

Interface exchange interactions. The Hamiltonian governing the Dirac fermions at the interface of a FMI/TI heterostructure has the general form

$$H_{\rm Dirac}(\mathbf{n}(\mathbf{r})) = [\mathbf{d}(-i\hbar\nabla) - J_0\mathbf{n}(\mathbf{r})]\cdot\sigma, \quad (1)$$

where $\mathbf{r}=(x,y)$, $\sigma=(\sigma_x,\sigma_y,\sigma_z)$ is a vector of Pauli matrices, and J_0 is the interface exchange coupling. The operator $\mathbf{d}$ is a function of the momentum operator $-i\hbar\nabla$. Here, we consider the two possibilities leading to a Dirac spectrum,

$$\mathbf{d}_1 = -i\hbar v_F\nabla, \quad \mathbf{d}_2 = -i\hbar v_F\nabla\times\hat{\mathbf{z}}, \quad (2)$$

with the latter arising in TIs such as Bi_2Se_3, Bi_2Te_3, and Sb_2Te_3 [26]. Experimentally, in order for the effective Hamiltonian (1) to give a valid low-energy description of the physics at the interface, the TI must be at least 7 nm thick. The end result will be that $\mathbf{d}_1$ induces a DMI of the type $\mathbf{n}\cdot(\nabla\times\mathbf{n})$, which is often referred to as a bulk DMI, but for clarity we call it a *Bloch DMI*. Instead, $\mathbf{d}_2$ leads to a different type of DMI, $\sim\mathbf{n}\cdot[(\hat{\mathbf{z}}\times\nabla)\times\mathbf{n}] = (\mathbf{n}\cdot\nabla)\mathrm{n}_z - \mathrm{n}_z(\nabla\cdot\mathbf{n})$, in the magnetic literature sometimes known as surface DMI, but to which we refer to as *Néel DMI*.

The effective energy $E_{\rm eff}$ of the system is obtained by integrating out the Dirac fermions $c=(c_\uparrow,c_\downarrow)$ in the partition function,

$$e^{-\beta E_{\rm eff}(\mathbf{n})} = e^{-\beta\rho_s L\int_S dS(\nabla\mathbf{n})^2} \times\int\mathcal{D}c^\dagger\mathcal{D}c\, e^{-\int_0^\beta d\tau\int d^2r c^\dagger[\partial_\tau-\mu+H_{\rm Dirac}(\mathbf{n}(\mathbf{r}))]c}, \quad (3)$$

where ρ_s is the magnetization stiffness of the FMI, L is the film thickness, and the integration is over the film area S. Due to the nonzero z component of the magnetization, the above model yields a gapped Dirac spectrum for $T<T_c$ with spin-wave excitations, which give rise to a Chern-Simons term [10]. However, this gap does not occur for $T>T_c$. In the following, we assume that the gap vanishes for $T\geqslant T_c$ and we obtain the corresponding corrections to the free energy after integrating out the gapless Dirac fermions.

Effective free energy and induced DMI. The noninteracting Green's function for a spin-momentum locked system can be written in general as

$$\mathcal{G}_{\alpha\beta}(\omega_n,\mathbf{k}) = G(\omega_n,\mathbf{k})\delta_{\alpha\beta} + \mathbf{F}(\omega_n,\mathbf{k})\cdot\sigma_{\alpha\beta}, \quad (4)$$

where $\omega_n=(2n+1)\pi/\beta$ is the fermionic Matsubara frequency.

From the Hamiltonian (1) and the functional integral in (3), we have

$$G(\omega_n,\mathbf{k}) = \frac{i\omega_n+\mu}{(i\omega_n+\mu)^2-\mathbf{d}^2(\mathbf{k})}, \quad (5)$$

$$\mathbf{F}(\omega_n,\mathbf{k}) = -\frac{\mathbf{d}(\mathbf{k})}{(i\omega_n+\mu)^2-\mathbf{d}^2(\mathbf{k})}, \quad (6)$$

where $\mathbf{d}(\mathbf{k})$ is either $\mathbf{d}_1$ or $\mathbf{d}_2$ from Eq. (2) in momentum space. Integrating out the fermions and expanding the free-energy expression up to J_0^2, we obtain, after a long but straightforward calculation, the following correction to the effective free-energy density [27],

$$\delta\mathcal{F}_{\rm Dirac}^{\rm mag} = \frac{s}{2}\{[\nabla\mathbf{n}(\mathbf{r})]^2 + [\nabla\cdot\mathbf{n}(\mathbf{r})]^2\} + i\frac{a}{2}\mathbf{n}(\mathbf{r})\cdot[\mathbf{d}(-i\hbar\nabla)\times\mathbf{n}(\mathbf{r})], \quad (7)$$

where $(\nabla\mathbf{n})^2 = \sum_{i=x,y,z}(\nabla\mathrm{n}_i)^2$ defines the usual exchange term, and we have defined $s=\beta J_0^2/[24\pi\cosh^2(\beta\mu/2)]$ and $a=J_0^2(8\pi\hbar v_F)^{-1}\tanh(\beta\mu/2)$. We can drop the constant term $F_{\rm Dirac}(0)$ from the free energy, since it does not depend on the field. Thus, we can safely write $\mathcal{F}_{\rm Dirac}=\delta\mathcal{F}_{\rm Dirac}$. The above expression features a DMI induced by Dirac fermion fluctuations. In addition, a contribution $\sim(\nabla\cdot\mathbf{n})^2$ is also generated. We will see below that the presence of this term leads to interesting physical properties when $\mathbf{d}_2$ is replaced for $\mathbf{d}$ in Eq. (7), modifying in this way the behavior of Néel skyrmions. Note that differently from the case where the Dirac fermion is gapped [15], no intrinsic anisotropy is generated by the Dirac fermions. At the same time, we note that the form of $\delta\mathcal{F}_{\rm Dirac}^{\rm mag}$ including the DMI term will persist also below T_c as long as the chemical potential is outside the gap, meaning that the TI surface is metallic, despite the generated mass m for the Dirac fermions.

Effective magnetic energy in an external field. The contributions from the FMI and Dirac fermions allow one to recast the effective energy for a thin ferromagnetic layer in the form

$$E_{\rm eff} = L\int_S\{A[(\nabla\mathbf{n})^2+\epsilon(\nabla\cdot\mathbf{n})^2] + D\mathscr{E}_{\rm DMI} + M_sH(1-\mathrm{n}_z)\}\mathrm{d}S, \quad (8)$$

where $A=\rho_s+s/(2L)$ is the effective magnetization stiffness including the fluctuations due to the Dirac fermions. We assumed that the sample lies in the presence of an external magnetic field H applied perpendicular to it. We have also introduced the parameter $\epsilon=s/(2AL)=s/(2\rho_sL+s)$. The DM coupling is given by $D=a/(2L)$. The DM interaction has the possible forms $\mathscr{E}_{\rm DMI}^{\rm B}=\mathbf{n}\cdot(\nabla\times\mathbf{n})$ or $\mathscr{E}_{\rm DMI}^{\rm N}=\mathrm{n}_z\nabla\cdot\mathbf{n}-\mathbf{n}\cdot\nabla\mathrm{n}_z$, depending on whether $\mathbf{d}_1$ or $\mathbf{d}_2$ arises in the Dirac Hamiltonian (1). The latter is more adequate for Bi_2Se_3-EuS samples [13]. The *ab initio* results from Ref. [28] indicate that J_0 is largely enhanced due to Ruderman-Kittel-Kasuya-Yosida (RKKY) interactions at the Bi_2Se_3-EuS interface, ranging from 35 to 40 meV. Using $J_0=35$ meV one can estimate that at room temperature $s\in[0.05,0.63)$ meV, and therefore $\epsilon\in[0.08,0.51)$ for a 1-nm-thick film and $\mu\in(0,0.1]$ eV [29]. Note that ϵ strongly depends on the value of μ, which can be reduced by doping.

Although the temperature fluctuations usually destroy skyrmions in thin films, the individual skyrmions [30–32] as well as skyrmion lattices [33] are observed in various multilayer structures for room temperatures. Therefore, in experiments, it is reasonable to use a multilayer structure in the form of the periodically repeated stack TI/FMI/NI, where NI is a normal insulator. In the following, we neglect the influence of the thermal fluctuations on the magnetization structure, which holds when model (8) is applied for a multilayer structure.

Before studying the energy functional (8), let us emphasize that while the DMI is absent for the case of a vanishing chemical potential, the term $(\nabla\cdot\mathbf{n})^2$ is always there, even if $\mu=0$. Thus, this term is a unique feature of thin-film FMIs proximate to a three-dimensional TI. In fact, it has been recently demonstrated that it is also induced for $\mu=0$ at zero temperature when the surface Dirac fermions are gapped by the proximity effect to the FMI [15].

Ground states of system (8) are well studied for the case $\epsilon = 0$ [34–38]. The uniform saturation along the field is the ground state with $E_{\text{eff}} = 0$ for large fields and weak DM interactions, and a one-dimensional (1D) structure in the form of a periodical sequence of 2π domain walls is the ground state with $E_{\text{eff}} < 0$ for small fields and strong DM interactions. The criterion for the periodical state appearance is negative energy of a single domain wall, which reads $d > d_c = 8/\pi$, where $d = \sqrt{2}D/\sqrt{AM_sH}$ is a dimensionless DM constant. In the vicinity of the boundary $d \approx d_c$, an intermediate phase in the form of a two-dimensional (2D) periodical structure (skyrmion lattice) forms the ground state [20,21,34,39]. An isolated skyrmion [21,22,35,40] may appear as a topologically stable excitation of the uniformly saturated state. The skyrmions and domain walls are of Bloch and Néel types for the DM interaction in the forms $\mathscr{E}_{\text{DMI}}^{\text{B}}$ and $\mathscr{E}_{\text{DMI}}^{\text{N}}$, respectively.

Here, we study how the ground states and individual skyrmions are changed when $\epsilon > 0$. Since $\boldsymbol{\nabla}\cdot\mathbf{n} \equiv 0$ for any domain wall and skyrmion of the Bloch type (induced by $\mathscr{E}_{\text{DMI}}^{\text{B}}$), the influence of the term $(\boldsymbol{\nabla}\cdot\mathbf{n})^2$ is not significant in this case. However, it drastically changes the ground-state diagram and stability of the static solutions for the case of $\mathscr{E}_{\text{DMI}}^{\text{N}}$. In this case, $d_c = d_c^{\text{N}}(\epsilon) = (8/\pi)\int_0^1 \sqrt{1+\epsilon(2\xi^2-1)^2}\, d\xi$ and the period of the 1D structure is increased with ϵ [27]. Energy per period is $E_{\text{1D}}^{\text{N}}(d,\epsilon) \approx AL\mathcal{E}(d,\epsilon)$, where $\mathcal{E}(d,\epsilon)$ is determined by the implicit relation $d/d_c^{\text{N}}(\epsilon) = \text{E}(4/\mathcal{E})\sqrt{-\mathcal{E}/4}$, with $\text{E}(k)$ being the complete elliptic integral of the second kind [41] (note that $\mathcal{E} < 0$). For the case $\mathscr{E}_{\text{DMI}}^{\text{B}}$ the 1D periodical structure is not affected by ϵ and one has $d_c^{\text{B}} = d_c^{\text{N}}(0)$ and $E_{\text{1D}}^{\text{B}}(d) = E_{\text{1D}}^{\text{N}}(d,0)$ [27].

Skyrmion solutions. Here, we consider the topologically stable excitations of the saturated state $\mathbf{n} = \hat{\mathbf{z}}$. First, we utilize the constraint $\mathbf{n}^2 = 1$ by expressing the direction of the magnetization in spherical coordinates, $\mathbf{n} = \sin\theta(\cos\phi\hat{\mathbf{x}} + \sin\phi\hat{\mathbf{y}}) + \cos\theta\hat{\mathbf{z}}$. One can show [27] that for the case $\mathscr{E}_{\text{DMI}}^{\text{N}}$ the total energy (8) has a local minimum if $\phi = \chi$ and function $\theta = \theta(\rho)$ is determined by the equation

$$(1+\epsilon\cos^2\theta)\nabla_\rho^2\theta - \sin\theta\cos\theta\left(\frac{1+\epsilon}{\rho^2} + \epsilon\theta'^2\right) + d\frac{\sin^2\theta}{\rho} - \sin\theta = 0, \tag{9}$$

where we introduced the polar frame of reference $\{\rho,\chi\}$ with the radial distance ρ measured in units of $\ell = \sqrt{2A/(M_sH)}$ and $\nabla_\rho^2 f = \rho^{-1}\partial_\rho(\rho\,\partial_\rho f)$ denotes the radial part of the Laplace operator. Equation (9) must be solved with the boundary conditions $\theta(0) = \pi$, $\theta(\infty) = 0$. A number of examples of skyrmion profiles determined by Eq. (9) for various values of parameters d and ϵ are shown in Fig. S2 [27]. Note that the skyrmion size is mainly determined by the parameter d, while the parameter ϵ weakly modifies the details of the skyrmion profile. For the case $\mathscr{E}_{\text{DMI}}^{\text{B}}$ the equilibrium solution is $\phi = \chi + \pi/2$ and the corresponding equation for the profile $\theta(\rho)$ coincides with (9) when $\epsilon = 0$. Note that in this case Eq. (9) is reduced to the well-known skyrmion equation [23,34,40].

In order to analyze the stability of the obtained static solutions we study the spectrum of the skyrmion eigenexcitations by means of the methods commonly applied for skyrmions [38,42] as well as for other two-dimensional magnetic topological solitons [43–47]. Namely, we introduce

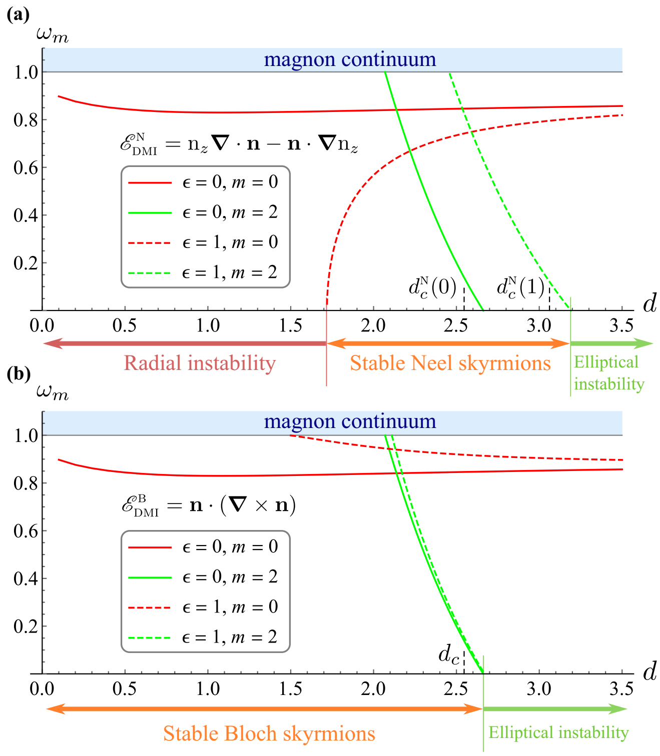

FIG. 1. Eigenfrequencies of two localized modes, namely, radially symmetric ($m = 0$) and elliptic ($m = 2$), are found by means of a numerical solution of the eigenvalue problem for different DM terms. Modes which do not demonstrate instability are not shown. Stability/instability regions are indicated for the case $\epsilon = 1$.

small, time-dependent deviations $\theta = \theta_0 + \vartheta$ and $\phi = \phi_0 + \varphi/\sin\theta_0$, where $\vartheta, \varphi \ll 1$ and $\theta_0 = \theta_0(\rho)$, and ϕ_0 denotes the static profile. The linearization of the Landau-Lifshitz equations, $\sin\theta\,\partial_t\phi = \frac{\gamma}{M_s}\delta E_{\text{eff}}/\delta\theta$, $-\sin\theta\,\partial_t\theta = \frac{\gamma}{M_s}\delta E_{\text{eff}}/\delta\phi$, in the vicinity of the static solution results in solutions for the deviations in the form $\vartheta = f(\rho)\cos(\omega\tau + m\chi + \chi_0)$, $\varphi = g(\rho)\sin(\omega\tau + m\chi + \chi_0)$, where $m \in \mathbb{Z}$ is an azimuthal quantum number and χ_0 is an arbitrary phase. Here, $\tau = t\Omega_0$ is the dimensionless time, where $\Omega_0 = \gamma H$ is the Larmor frequency with γ being the gyromagnetic ratio. The eigenfrequencies ω and the corresponding eigenfunctions f, g are determined by solving the Bogoliubov–de Gennes eigenvalue problem [27]. The numerical solution was obtained for a range of d and a couple of values of ϵ. A number of bounded eigenmodes with $\omega < 1$ are found in the gap. Eigenfrequencies of the radially symmetric ($m = 0$) and elliptic ($m = 2$) modes are shown in Fig. 1, where we compare both types of DM terms [48]. If $\epsilon = 0$, the spectra are identical for both cases, in particular, the well-known elliptical instability [35,38] takes place due to the softening of the elliptic mode in the region $d > d_c$, where the uniformly saturated state is thermodynamically unstable [38]. For the case $\mathscr{E}_{\text{DMI}}^{\text{N}}$ the ϵ term shifts the elliptical instability to the larger values of d with the condition $d > d_c^{\text{N}}(\epsilon)$ kept, while in the case $\mathscr{E}_{\text{DMI}}^{\text{B}}$ the effect of the ϵ term is negligible.

Remarkably, the ϵ term influences oppositely on the breathing mode ($m = 0$), for different DM types. For the case $\mathscr{E}_{\text{DMI}}^{\text{B}}$ the eigenfrequency ω_0 is increased and for small d the breathing mode is pushed out from the gap into the magnon continuum. As a result, the small-radius skyrmions are free of the bounded states. This is in contrast to the case $\mathscr{E}^{\rm N}_{\rm DMI}$, when the breathing mode eigenfrequency is rapidly decreased, resulting in a radial instability for small d. In order to give some physical insight into the latter effect, we consider the model where the skyrmion profile is described by the linear ansatz [23,34] $\theta_{\rm a}(\rho)=\frac{\pi}{R}(R-\rho){\rm H}(R-\rho)$, and $\phi=\chi+\Phi$. Here, the variational parameters R and Φ describe the skyrmion radius and helicity, respectively, and ${\rm H}(x)$ is the Heaviside step function. For this model, total energy (8) with $\mathscr{E}_{\rm DMI}=\mathscr{E}^{\rm N}_{\rm DMI}$ reads

$$\frac{E^{\rm N}_{\rm tot}}{2\pi AL}=e_{\rm ex}+\epsilon e_\epsilon\cos^2\Phi-2\delta\cos\Phi R+R^2e_{\rm H},\quad(10)$$

where the constants $e_{\rm ex}\approx 6.15$ [49], $e_\epsilon=e_{\rm ex}-\pi^2/4$, and $e_{\rm H}=1-4/\pi^2$ originate from the exchange, ϵ-term, and Zeeman contributions, respectively. Here, $\delta=d\pi/4$. The energy expression (10) shows that the equilibrium helicity Φ is determined by the competition of the ϵ term, which tends to $\Phi=\pm\pi/2$ (Bloch skyrmion), and the DM term, which tends to $\Phi=0$ (Néel skyrmion). At the same time, the equilibrium skyrmion radius is determined by the competition of the DM and Zeeman terms, and for the Bloch skyrmion one has $R=0$. Thus, the skyrmion collapse is expected with the ϵ increasing. Indeed, the minimization of the total energy (10) with respect to the both variational parameters results in the critical value $\epsilon_c=\delta^2/(e_\epsilon e_{\rm H})$: If $\epsilon<\epsilon_c$, then the equilibrium values of the variational parameters $R_0=\delta/e_{\rm H}$ and $\Phi_0=0$ determine the Néel skyrmion; if $\epsilon>\epsilon_c$, the minimum of energy (10) is reached for $R_0=0$ and $\Phi_0=\pm\pi/2$. The latter corresponds to a collapsed Bloch skyrmion. In other words, a stable Néel slyrmion exists for the case $\epsilon<\epsilon_c$. Surprisingly, there are no intermediate states with $0<\Phi_0<\pi/2$ when $\epsilon>\epsilon_c$.

Skyrmion lattice. In order to estimate the region of existence of the skyrmion lattice we use the circular cell approximation [34], when the lattice cell is approximated by a circle of radius R and the boundary condition $\theta(R)=0$ is applied. The skyrmion profile is described by the same linear ansatz as for the case of an isolated skyrmion. Minimizing the energy (10) per unit cell $E^{\rm N}_{\rm 2D}=E^{\rm N}_{\rm tot}/(\pi R^2)$, one obtains the following equilibrium values of the variational parameters $\Phi^{\rm N}_0=0$, $R^{\rm N}_0(\epsilon)=(e_{\rm ex}+\epsilon e_\epsilon)/\delta$, and the corresponding equilibrium energy reads $E^{\rm N}_{\rm 2D}(\epsilon)=2AL[e_{\rm H}-\delta^2/(e_{\rm ex}+\epsilon e_\epsilon)]$. For the case $\mathscr{E}^{\rm B}_{\rm DMI}$ the same procedure results in the ϵ-independent values $\Phi^{\rm B}_0=\pi/2$, $R^{\rm B}_0=R^{\rm N}_0(0)$, and $E^{\rm B}_{\rm 2D}=E^{\rm N}_{\rm 2D}(0)$.

Comparing the energies of three states, namely, the energy of the uniform magnetization along field $E=0$, energy of the 1D periodical state (per period) $E_{\rm 1D}$, and energy of the skyrmion lattice per unit cell $E_{\rm 2D}$, we determine the phase diagram of the ground states (see Fig. 2). Note that for $\epsilon>\epsilon_0\approx 0.98$ the skyrmion lattice is not a ground state. Given the dependence of ϵ with the exchange coupling J_0, temperature, and chemical potential, the skyrmion lattice phase is likely to occur for a not too high-temperature range as compared to the Curie temperature of EuS. The dimensionless DM parameter d can then be tuned by the external field to attain the interval shown under the green area of Fig. 2(a).

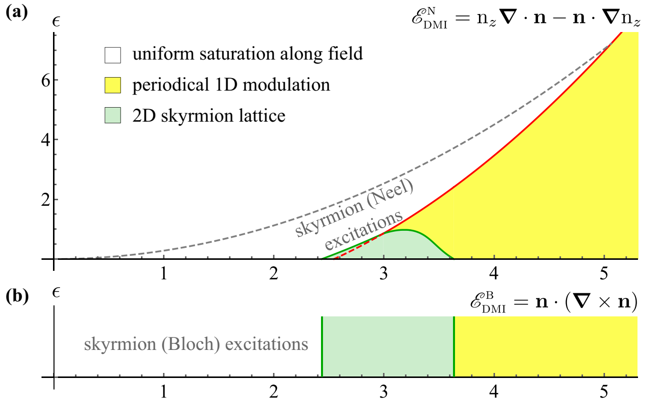

FIG. 2. Diagrams of the ground states for different kinds of DMI. (a) The red line is determined by the condition $d=d^{\rm N}_c(\epsilon)$, which separates the uniform state and periodical 1D modulation. The green region of the Néel skyrmion lattices is determined by the conditions $E^{\rm N}_{\rm 2D}<E^{\rm N}_{\rm 1D}$ and $E^{\rm N}_{\rm 2D}<0$ to the right and to the left of the red line. The gray dashed line is the line of collapse of the Néel skyrmions, which is determined by the condition $\epsilon=\epsilon_c(d)$. (b) Colors have the same meaning as in (a), but periodical helical state and skyrmion lattices are of Bloch type. The excitations in the form of isolated Bloch skyrmions are stable within the all-white region. If $\mathbf{d}_1$ is used in the Hamiltonian (1), the coefficient of the $(\nabla\cdot\mathbf{n})^2$ would be negative, which would in turn make the Bloch skyrmion more stable.

Conclusions. We have shown that the effective magnetic energy for a TI-FMI heterostructure exhibits a Dzyaloshinskii-Moriya term induced by tracing out the surface Dirac fermions proximate to the FMI. A unique feature of the effective energy as compared to other DM systems is the presence of an additionally induced magnetic capacitance energy, given by a term proportional to the square of the magnetic charge $\nabla\cdot\mathbf{n}$. Despite having a small magnitude in realistic samples, the interplay between this term and the DM one yields a phase diagram with interesting phase boundaries in the case of a Néel DMI, which is the situation relevant for, e.g., Bi_2Se_3 samples proximate to a FMI. Our theory is directly relevant for very recently synthesized TI-ferromagnetic thin-film heterostructures, in some of which the formation of a skyrmionic magnetic texture has been observed [19].

Acknowledgments. F.S.N. and I.E. thank the DFG Priority Program SPP 1666, "Topological Insulators," under Grant No. ER 463/9. J.v.d.B. acknowledges support from SFB 1143. F.K. and J.S.M. acknowledge the support from NSF Grants No. DMR-1207469 and No. 1700137, ONR Grants No. N00014-13-1-0301 and No. N00014-16-1-2657, and the STC Center for Integrated Quantum Materials under NSF Grant No. DMR-1231319. F.K. acknowledges the Science and Technological Research Council of Turkey (TUBITAK) through the BIDEB 2232 Program under Award No. 117C050 (Low-Dimensional Hybrid Topological Materials). I.E. acknowledges support by the Ministry of Education and Science of the Russian Federation in the framework of Increase Competitiveness Program of NUST MISiS (Grant No. K2-2017-085).

[1] M. Z. Hasan and C. L. Kane, Colloquium: Topological insulators, Rev. Mod. Phys. **82**, 3045 (2010).

[2] X.-L. Qi and S.-C. Zhang, Topological insulators and superconductors, Rev. Mod. Phys. **83**, 1057 (2011).

[3] S. Deser, R. Jackiw, and S. Templeton, Three-Dimensional Massive Gauge Theories, Phys. Rev. Lett. **48**, 975 (1982); A. J. Niemi and G. W. Semenoff, Axial-Anomaly-Induced Fermion Fractionization and Effective Gauge-Theory Actions in Odd-Dimensional Space-Times, *ibid.* **51**, 2077 (1983); A. N. Redlich, Parity violation and gauge noninvariance of the effective gauge field action in three dimensions, Phys. Rev. D **29**, 2366 (1984).

[4] X.-L. Qi, T. L. Hughes, and S.-C. Zhang, Topological field theory of time-reversal invariant insulators, Phys. Rev. B **78**, 195424 (2008).

[5] F. Katmis, V. Lauter, F. S. Nogueira, B. A. Assaf, M. E. Jamer, P. Wei, B. Satpati, J. W. Freeland, I. Eremin, D. Heiman, P. Jarillo-Herrero, and J. S. Moodera, A high-temperature ferromagnetic topological insulating phase by proximity coupling, Nature (London) **533**, 513 (2016).

[6] P. Wei, F. Katmis, B. A. Assaf, H. Steinberg, P. Jarillo-Herrero, D. Heiman, and J. S. Moodera, Exchange-Coupling-Induced Symmetry Breaking in Topological Insulators, Phys. Rev. Lett. **110**, 186807 (2013).

[7] I. Garate and M. Franz, Inverse Spin-Galvanic Effect in the Interface between a Topological Insulator and a Ferromagnet, Phys. Rev. Lett. **104**, 146802 (2010).

[8] T. Yokoyama, J. Zang, and N. Nagaosa, Theoretical study of the dynamics of magnetization on the topological surface, Phys. Rev. B **81**, 241410(R) (2010).

[9] Y. Tserkovnyak and D. Loss, Thin-Film Magnetization Dynamics on the Surface of a Topological Insulator, Phys. Rev. Lett. **108**, 187201 (2012).

[10] F. S. Nogueira and I. Eremin, Fluctuation-Induced Magnetization Dynamics and Criticality at the Interface of a Topological Insulator with a Magnetically Ordered Layer, Phys. Rev. Lett. **109**, 237203 (2012).

[11] F. S. Nogueira and I. Eremin, Semimetal-insulator transition on the surface of a topological insulator with in-plane magnetization, Phys. Rev. B **88**, 085126 (2013).

[12] Y. Tserkovnyak, D. A. Pesin, and D. Loss, Spin and orbital magnetic response on the surface of a topological insulator, Phys. Rev. B **91**, 041121(R) (2015).

[13] M. Li, W. Cui, J. Yu, Z. Dai, Z. Wang, F. Katmis, W. Guo, and J. Moodera, Magnetic proximity effect and interlayer exchange coupling of ferromagnetic/topological insulator/ferromagnetic trilayer, Phys. Rev. B **91**, 014427 (2015).

[14] S. Rex, F. S. Nogueira, and A. Sudbø, Nonlocal topological magnetoelectric effect by coulomb interaction at a topological insulator-ferromagnet interface, Phys. Rev. B **93**, 014404 (2016).

[15] S. Rex, F. S. Nogueira, and A. Sudbø, Topological magnetic dipolar interaction and nonlocal electric magnetization control in topological insulator heterostructures, Phys. Rev. B **94**, 020404(R) (2016).

[16] Q. I. Yang, M. Dolev, L. Zhang, J. Zhao, A. D. Fried, E. Schemm, M. Liu, A. Palevski, A. F. Marshall, S. H. Risbud, and A. Kapitulnik, Emerging weak localization effects on a topological insulator–insulating ferromagnet (Bi_2Se_3-EuS) interface, Phys. Rev. B **88**, 081407(R) (2013).

[17] C. Lee, F. Katmis, P. Jarillo-Herrero, J. S. Moodera, and N. Gedik, Direct measurement of proximity-induced magnetism at the interface between a topological insulator and a ferromagnet, Nat. Commun. **7**, 12014 (2016).

[18] C. Tang, C.-Z. Chang, G. Zhao, Y. Liu, Z. Jiang, C.-X. Liu, M. R. McCartney, D. J. Smith, T. Chen, J. S. Moodera, and J. Shi, Above 400-K robust perpendicular ferromagnetic phase in a topological insulator, Sci. Adv. **3**, e1700307 (2017).

[19] S. Zhang, F. Kronast, G. van der Laan, and T. Hesjedal, Real-space observation of skyrmionium in a ferromagnet-magnetic topological insulator heterostructure, Nano Lett. **18**, 1057 (2018).

[20] N. Nagaosa and Y. Tokura, Topological properties and dynamics of magnetic skyrmions, Nat. Nanotechnol. **8**, 899 (2013).

[21] A. Fert, N. Reyren, and V. Cros, Magnetic skyrmions: Advances in physics and potential applications, Nat. Rev. Mater. **2**, 17031 (2017).

[22] R. Wiesendanger, Nanoscale magnetic skyrmions in metallic films and multilayers: A new twist for spintronics, Nat. Rev. Mater. **1**, 16044 (2016).

[23] A. N. Bogdanov and D. A. Yablonskiĭ, Thermodynamically stable "vortices" in magnetically ordered crystals. the mixed state of magnets, Zh. Eksp. Teor. Fiz. **95**, 178 (1989) [Sov. Phys. JETP **68**, 101 (1989)].

[24] In contrast to the weak contribution from the nonlocal energy of the volume magnetostatic charges, which for a thin film scales quadratically with the thickness, the considered "magnetic charging energy" is linear with the thickness and, therefore, it cannot be neglected.

[25] D. Andrikopoulos and B. Sorée, Skyrmion electrical detection with the use of three-dimensional topological insulators/ferromagnetic bilayers, Sci. Rep. **7**, 17871 (2017).

[26] C.-X. Liu, X.-L. Qi, H. Zhang, X. Dai, Z. Fang, and S.-C. Zhang, Model Hamiltonian for topological insulators, Phys. Rev. B **82**, 045122 (2010).

[27] See Supplemental Material at http://link.aps.org/supplemental/10.1103/PhysRevB.98.060401 for technical details, including the derivation of the free energy density, calculation of magnetization structures and the analysis of their stability.

[28] J. Kim, K.-W. Kim, H. Wang, J. Sinova, and R. Wu, Understanding the Giant Enhancement of Exchange Interaction in Bi_2Se_3-EuS Heterostructures, Phys. Rev. Lett. **119**, 027201 (2017).

[29] For EuS we would have $\rho_s = \mathcal{S}^2[J_1 + J_2/2]/a_0 \approx 0.29$ meV/nm, where $\mathcal{S} = 7/2$ is the spin of the Eu atom, $J_1/k_B = 0.228$ K and $J_2/k_B = -0.118$ K are the nearest- and next-nearest-neighbor exchange energies, respectively, and for the lattice spacing $a_0 = 5.968$ Å [50].

[30] C. Moreau-Luchaire, C. Moutafis, N. Reyren, J. Sampaio, C. A. F. Vaz, N. Van Horne, K. Bouzehouane, K. Garcia, C. Deranlot, P. Warnicke, P. Wohlhuter, J.-M. George, M. Weigand, J. Raabe, V. Cros, and A. Fert, Additive interfacial chiral interaction in multilayers for stabilization of small individual skyrmions at room temperature, Nat. Nanotechnol. **11**, 444 (2016).

[31] A. Soumyanarayanan, M. Raju, A. L. G. Oyarce, A. K. C. Tan, M.-Y. Im, A. P. Petrović, P. Ho, K. H. Khoo, M. Tran, C. K. Gan, F. Ernult, and C. Panagopoulos, Tunable room-temperature magnetic skyrmions in Ir/Fe/Co/Pt multilayers, Nat. Mater. **16**, 898 (2017).

[32] O. Boulle, J. Vogel, H. Yang, S. Pizzini, D. de Souza Chaves, A. Locatelli, T. O. Menteş, A. Sala, L. D. Buda-Prejbeanu, O. Klein, M. Belmeguenai, Y. Roussigné, A. Stashkevich, S. M. Chérif, L. Aballe, M. Foerster, M. Chshiev, S. Auffret, I. M. Miron, and G. Gaudin, Room-temperature chiral magnetic skyrmions in ultrathin magnetic nanostructures, Nat. Nanotechnol. **11**, 449 (2016).

[33] S. Woo, K. Litzius, B. Kruger, M.-Y. Im, L. Caretta, K. Richter, M. Mann, A. Krone, R. M. Reeve, M. Weigand, P. Agrawal, I. Lemesh, M.-A. Mawass, P. Fischer, M. Klaui, and G. S. D. Beach, Observation of room-temperature magnetic skyrmions and their current-driven dynamics in ultrathin metallic ferromagnets, Nat. Mater. **15**, 501 (2016).

[34] A. Bogdanov and A. Hubert, Thermodynamically stable magnetic vortex states in magnetic crystals, J. Magn. Magn. Mater. **138**, 255 (1994).

[35] A. Bogdanov and A. Hubert, The properties of isolated magnetic vortices, Phys. Status Solidi B **186**, 527 (1994).

[36] A. Bogdanov and A. Hubert, The stability of vortex-like structures in uniaxial ferromagnets, J. Magn. Magn. Mater. **195**, 182 (1999).

[37] M. N. Wilson, A. B. Butenko, A. N. Bogdanov, and T. L. Monchesky, Chiral skyrmions in cubic helimagnet films: The role of uniaxial anisotropy, Phys. Rev. B **89**, 094411 (2014).

[38] C. Schütte and M. Garst, Magnon-skyrmion scattering in chiral magnets, Phys. Rev. B **90**, 094423 (2014).

[39] U. K. Rößler, A. N. Bogdanov, and C. Pfleiderer, Spontaneous skyrmion ground states in magnetic metals, Nature (London) **442**, 797 (2006).

[40] A. O. Leonov, T. L. Monchesky, N. Romming, A. Kubetzka, A. N. Bogdanov, and R. Wiesendanger, The properties of isolated chiral skyrmions in thin magnetic films, New J. Phys. **18**, 065003 (2016).

[41] M. Abramowitz and I. A. Stegun, *Handbook of Mathematical Functions with Formulas, Graphs, and Mathematical Tables*, 9th Dover ed., 10th GPO ed. (Dover, New York, 1972).

[42] V. P. Kravchuk, D. D. Sheka, U. K. Rößler, J. van den Brink, and Y. Gaididei, Spin eigenmodes of magnetic skyrmions and the problem of the effective skyrmion mass, Phys. Rev. B **97**, 064403 (2018).

[43] B. A. Ivanov, H. J. Schnitzer, F. G. Mertens, and G. M. Wysin, Magnon modes and magnon-vortex scattering in two-dimensional easy-plane ferromagnets, Phys. Rev. B **58**, 8464 (1998).

[44] D. D. Sheka, B. A. Ivanov, and F. G. Mertens, Internal modes and magnon scattering on topological solitons in two-dimensional easy-axis ferromagnets, Phys. Rev. B **64**, 024432 (2001).

[45] D. D. Sheka, I. A. Yastremsky, B. A. Ivanov, G. M. Wysin, and F. G. Mertens, Amplitudes for magnon scattering by vortices in two-dimensional weakly easy-plane ferromagnets, Phys. Rev. B **69**, 054429 (2004).

[46] B. A. Ivanov and D. D. Sheka, Local magnon modes and the dynamics of a small–radius two–dimensional magnetic soliton in an easy-axis ferromagnet, JETP Lett. **82**, 436 (2005).

[47] D. D. Sheka, C. Schuster, B. A. Ivanov, and F. G. Mertens, Dynamics of topological solitons in two-dimensional ferromagnets, Eur. Phys. J. B **50**, 393 (2006).

[48] The stability analysis was performed for zero temperature. However, thermally induced magnons would only result in additional damping for bounded skyrmion modes.

[49] The exact value is $e_{\text{ex}} = [\pi^2 + \gamma_0 - \text{Ci}(2\pi) + \ln(2\pi)]/2$, where γ_0 is the Euler constant and $\text{Ci}(x)$ denotes the cosine integral function (see Ref. [34]).

[50] A. Mauger and C. Godart, The magnetic, optical, and transport properties of representatives of a class of magnetic semiconductors: The europium chalcogenides, Phys. Rep. **141**, 51 (1986).